IEEE Access
Multidisciplinary | Rapid Review | Open Access Journal

Received February 23, 2021, accepted April 2, 2021, date of publication April 6, 2021, date of current version April 23, 2021.

Digital Object Identifier 10.1109/ACCESS.2021.3071415

Passivity-Based Control Strategy With Improved Robustness for Single-Phase Three-Level T-Type Rectifiers

HASAN KOMURCUGIL[1], (Senior Member, IEEE), SERTAC BAYHAN[2], (Senior Member, IEEE), AND MARIUSZ MALINOWSKI[3], (Fellow, IEEE)

[1]Department of Computer Engineering, Eastern Mediterranean University, Famagusta, Famagusta 996628, Turkey
[2]Qatar Environment and Energy Research Institute, Hamad Bin Khalifa University, Doha, Qatar
[3]Institute of Control and Industrial Electronics, Warsaw University of Technology, 00-662 Warsaw, Poland

Corresponding author: Sertac Bayhan (sbayhan@hbku.edu.qa)

This work was supported in part by the Open Access Funding is provided by the Qatar National Library, and in part by the Qatar National Research Fund (a member of Qatar Foundation) under Grant NPRP12S-0214-190083.

ABSTRACT A passivity-based control (PBC) strategy with improved robustness for single-phase three-level rectifiers feeding resistive and constant power loads (CPLs) is proposed. It is shown that the control of the rectifier can be achieved if the damping injection is applied to the grid current only. In this case, the knowledge of load resistance is required in the computation of reference grid current amplitude. Since the output voltage and load current are dc quantities, the load resistance can be estimated easily. Then, the amplitude of the reference grid current is calculated from the power balance equation of the rectifier. The transfer function from reference grid current to actual grid current is derived. The derived transfer function is analyzed under variations in the filter inductance. The results reveal that the proposed PBC offers strong robustness to variations in the filter inductance when a suitable damping gain is selected. The performances of the proposed PBC strategy under undistorted and distorted grid voltage as well as, variations in inductor are investigated via experimental studies during steady-state and transients caused by the resistive load and CPL changes. In all cases, the output voltage is regulated at the desired value, and grid current tracks its reference.

INDEX TERMS Passivity-based control, damping injection, three-level T-type rectifier, constant power load.

I. INTRODUCTION

Due to the well-known features such as controllable dc-link voltage, sinusoidal grid current with reasonably small total harmonic distortion (THD), bidirectional power flow capability and ability of unity power factor operation, the pulse width modulation (PWM) rectifiers are widely used in many applications such as motor drives [1], energy storage systems [2], renewable power generation systems [3], microgrids [4], and battery charger in hybrid electric vehicles [5]. In the last decade, multilevel converters are investigated as highly competitive topology to the conventional two-level converters in terms of cost and efficiency [6], [7]. The harmonics generated in multilevel converters are much smaller than that of two-level converters for the same switching frequency. This implies that multilevel converters can achieve the same voltage (or current) quality by using smaller passive components compared to two-level converters. Among the multilevel converter topologies, the three-level T-type converter has important advantages such as reduced component count, highest post fault operation capability, and lower losses. Especially, these advantages are meaningful in low voltage applications if the efficiency and cost are important [8], [9]. Therefore, the three-level T-type rectifiers received significant attention from the researchers [10]–[18].

In [10]–[13], open-switch fault detection and tolerance control techniques are proposed to enhance the reliability of the T-type rectifier. Another important aspect that should be studied is the control of three-level T-type rectifiers. So far, there are only a few papers investigating the control of T-type rectifiers [14]–[18]. In [14], the authors introduced a model predictive control (MPC) method for single-phase

The associate editor coordinating the review of this manuscript and approving it for publication was Zhehan Yi.

This work is licensed under a Creative Commons Attribution 4.0 License. For more information, see https://creativecommons.org/licenses/by/4.0/

T-type rectifiers with observer ability. However, MPC suffers from the high computation burden in practice. In addition, the switching frequency is time-varying. Even though the switching frequency is constant in [15], the performance of the closed-loop system can be deteriorated under parameter variations due to the sensitivity of MPC on the parameters. As a remedy to the sensitivity to parameter variations, a sliding mode control (SMC) is proposed for T-type rectifiers [16], [17]. Even though the SMC has strong robustness to parameter variations, the chattering and time-varying switching frequency are the main drawbacks. Recently, a passivity-based control (PBC) is studied for single-phase T-type rectifiers [18]. However, the influence of parameter variations is not studied. Also, the proposed PBC method is not verified through experimental results.

On the other hand, the control methods presented in [14]–[18] are designed when the rectifier feeds a resistive load only. The performance of these control methods under constant power load (CPL) is not considered. Hence, in order to achieve constant power consumption, the load bus voltage increases as the CPL current decreases and vice versa [19], [20]. This phenomenon is known as the negative resistance characteristic of CPL, which deteriorates the damping of the system leading to instability of the closed-loop system. Therefore, the operation and control of T-type rectifiers are challenging, particularly when the rectifier feeds not only a resistive load, but also a CPL. A tightly regulated power electronic converter such as a DC/AC inverter and DC/DC converter connected to the load bus behaves like a CPL.

In this study, a PBC with an improved robustness feature is proposed for single-phase three-level T-type rectifiers feeding resistive load and CPL. PBC is recognized as one of the robust nonlinear control methods widely employed in controlling power converters. In the PBC design, the dynamic model of the system under consideration should be derived. Then, the type of required damping injection which will accomplish the desired control objectives can be determined from this model. In this study, it is shown that the control of dc output voltage and grid current can be achieved if the damping injection is applied to the grid current only. The equivalent resistance of the load, which contains a resistive load connected in parallel with a CPL can be estimated by using Ohm's law. The reference grid current amplitude is calculated from an equation that is derived from the power balance equation of the rectifier. The proposed PBC strategy possesses the following features:

i) It exhibits excellent steady-state and dynamic performances under load and reference changes,
ii) Despite the use of inductance L in the switching function, the proposed PBC offers strong robustness against variations in L with suitably adjusted damping gain,
iii) It stabilizes the system when $R > R_{CPL}$,
iv) It requires only one controller gain (damping gain), which leads to simplification in the implementation.

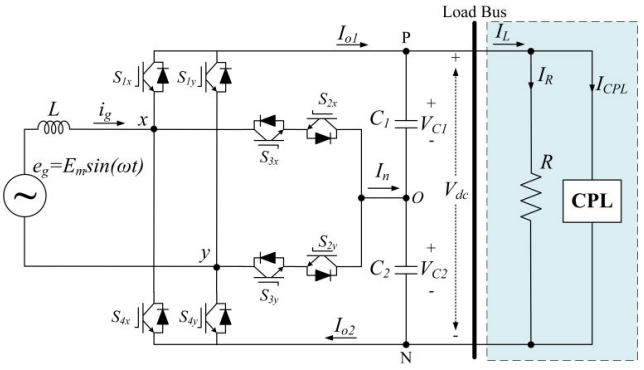

FIGURE 1. Single-phase three-level T-type rectifier feeding resistive load and CPL.

Experimental results obtained from a prototype are presented to validate the effectiveness of the proposed PBC strategy.

II. PROBLEM STATEMENT AND OPERATING STATES

The circuit diagram of a single-phase three-level T-type rectifier feeding the resistive load and CPL is depicted in Fig. 1. Clearly, there are four switches for each rectifier leg. The grid voltage (e_g) is connected to the rectifier via an inductance (L) whose resistance is represented by r. The load bus consists of parallel-connected resistive load (R) and CPL, which share I_L. The grid current passing through L is denoted by i_g. The dc-side variables are the rectifier current (I_{o1} and I_{o2}), load current (I_L), resistive load current (I_R), CPL current (I_{CPL}), neutral current (I_n), output voltage (V_{dc}), and capacitor voltages (V_{C1} and V_{C2}). The operation of the rectifier can be described by the following equations

$$e_g = L\frac{di_g}{dt} + v_{xy} \tag{1}$$

$$C_1\frac{dV_{C1}}{dt} = I_{o1} - \frac{V_{dc}}{R_L} \tag{2}$$

$$\frac{dV_{dc}}{dt} = \frac{2}{C_1}\left(I_{o1} - \frac{V_{dc}}{R} - \frac{P_{CPL}}{V_{dc}}\right) \tag{3}$$

where v_{xy} denotes the five-level voltage defined as $v_{xy} = uV_{dc}$, u denotes the switching function, R_L denotes the equivalent resistance of the entire load connected to the load bus (R and CPL), $I_{o1} = ui_g$, and P_{CPL} is the power of CPL. When V_{C1} and V_{C2} are balanced, the voltage across each capacitor is equal half of the dc output voltage ($V_{C1} = V_{C2} = V_{dc}/2$). It is worth noting that equation (3) is derived based on this fact. The CPL exhibits negative incremental resistance defined as follows

$$R_{CPL} = \frac{dV_{dc}}{dI_{CPL}} = \frac{d(\frac{P_{CPL}}{I_{CPL}})}{dI_{CPL}} = -\frac{P_{CPL}}{I_{CPL}^2} = -R_{inc} \tag{4}$$

Now, rewriting (3) using R_{CPL} yields

$$\frac{dV_{dc}}{dt} + \frac{2}{C_1}\left(\frac{R_{CPL} - R}{R_{CPL}R}\right)V_{dc} = \frac{2I_{o1}}{C_1} \tag{5}$$

The solution of (5) is given by

$$V_{dc} = I_{o1}\left(\frac{R_{CPL}R}{R_{CPL} - R}\right) - I_{o1}\left(\frac{R_{CPL}R}{R_{CPL} - R}\right)e^{-\frac{t}{\tau}} \tag{6}$$

where τ is given by

$$\tau = \frac{R_{CPL}RC_1}{2(R_{CPL} - R)} \tag{7}$$

Clearly, without a suitable closed-loop controller, V_{dc} does not converge to a stable solution when $R > R_{CPL}$ and the rectifier is destabilized under this loading condition.

On the other hand, unlike the traditional two-level rectifiers, the three-level T-type rectifier consists of four switches on each leg where two of them are anti-series connected between each leg and node O. With proper switching, this rectifier topology is able to produce three pole voltages (v_{kO} , $k = x, y$) with respect to node O. From Fig. 1, one can see that these voltages can be produced when the point x (or y) is connected to positive (P), neutral (O), and negative (N) points. Table 1 contains the operating states, switching states and pole voltages produced in each switching state. It is evident that the rectifier is in the P state producing $v_{kO} = +V_{dc}/2$ when the switches $S_{1k} = S_{2k} =$ ON and $S_{3k} = S_{4k} =$ OFF. The rectifier is in the O state producing 0V when $S_{2k} = S_{3k} =$ ON and $S_{1k} = S_{4k} =$ OFF. Finally, the rectifier is in the N state when $S_{3k} = S_{4k} =$ ON and $S_{1k} = S_{2k} =$ OFF producing $v_{kO} = -V_{dc}/2$. The five-level voltage v_{xy} can be expressed in terms of pole voltages of each leg as follows

$$v_{xy} = v_{xO} - v_{yO} \tag{8}$$

In [15], it is pointed out that there are nine switching states which yield five different voltage levels (0, $\pm V_{dc}/2$, and $\pm V_{dc}$) for v_{xy}.

TABLE 1. Operating states, switching states and pole voltages.

Operating State	S_{1k}	S_{2k}	S_{3k}	S_{4k}	v_{kO}
P	ON	ON	OFF	OFF	$+V_{dc}/2$
O	OFF	ON	ON	OFF	0
N	OFF	OFF	ON	ON	$-V_{dc}/2$

III. PASSIVITY-BASED CONTROL STRATEGY WITH IMPROVED ROBUSTNESS

A. PASSIVITY-BASED CONTROL

The main objectives in designing PBC for the single-phase rectifier include dc output voltage regulation, good ac current tracking, and unity power factor operation. The state variables are defined as the error in i_g and V_{dc} as follows

$$x_1 = i_g - i_g^*, \quad x_2 = V_{dc} - V_{dc}^* \tag{9}$$

where $i_g^* = I_m^* \sin(\omega t)$ denotes grid current reference with I_m^* being the reference amplitude and V_{dc}^* denotes the output voltage reference. Substituting $i_g = x_1 + i_g^*$ and $V_{dc} = x_2 + V_{dc}^*$ into (1) and (2), we obtain

$$L\dot{x}_1 + ux_2 = e_g - \left(L\frac{di_g^*}{dt} + uV_{dc}^*\right) \tag{10}$$

$$\frac{1}{2}\left(C_1\dot{x}_2 + \frac{x_2}{R_L}\right) = ux_1 + ui_g^* - \left(C_1\frac{dV_{dc}^*}{dt} + \frac{V_{dc}^*}{R_L}\right) \tag{11}$$

where $\dot{x}_1$ and $\dot{x}_2$ denote derivative of x_1 and x_2, respectively. In PBC, the damping injection is essential to achieve a stable operation [21], [22]. Now, adding damping terms ($\varsigma_1 x_1$ and $\varsigma_2 x_2$) to both sides of (10) and (11) results in

$$L\dot{x}_1 + ux_2 + \varsigma_1 x_1 = e_g - \left(L\frac{di_g^*}{dt} + uV_{dc}^* - \varsigma_1 x_1\right) \tag{12}$$

$$\frac{C_1\dot{x}_2}{2} + \frac{x_2}{R_L} + \varsigma_2 x_2 = ux_1 + ui_g^* - \left(\frac{C_1}{2}\frac{dV_{dc}^*}{dt} + \frac{V_{dc}^*}{R_L} - \varsigma_2 x_2\right) \tag{13}$$

where ς_1 and ς_2 are positive damping gains. In order to have a damping injection, the right-hand sides of (12) and (13) should be zero. In this case, we obtain

$$e_g = L\frac{di_g^*}{dt} + uV_{dc}^* - \varsigma_1 x_1 \tag{14}$$

$$ui_g^* = \frac{C_1}{2}\frac{dV_{dc}^*}{dt} + \frac{V_{dc}^*}{R_L} - \varsigma_2 x_2 \tag{15}$$

$$L\dot{x}_1 + ux_2 + \varsigma_1 x_1 = 0 \tag{16}$$

$$\frac{C_1\dot{x}_2}{2} + \frac{x_2}{R_L} + \varsigma_2 x_2 - ux_1 = 0 \tag{17}$$

The switching function u can be solved from (14) as follows

$$u = \frac{1}{V_{dc}^*}\left(e_g - L_e\frac{di_g^*}{dt} + \varsigma_1 x_1\right) \tag{18}$$

where L_e is the estimated value of actual L in the system. It is important to note that estimated values are not equal to the actual values in practice. Therefore, the influence of such parameter mismatch on the performance of the proposed control strategy should be investigated. Also, it is worth noting that the switching function in (18) does not involve output voltage feedback and damping gain ς_2. Thus, the control of V_{dc} is achieved indirectly by controlling i_g (see section III-E).

B. ROBUSTNESS IMPROVEMENT WITH DAMPING GAIN

Substituting the switching function u shown in (18) into (1) yields

$$e_g = L\frac{di_g}{dt} + \frac{V_{dc}}{V_{dc}^*}e_g - \frac{V_{dc}}{V_{dc}^*}L_e\frac{di_g^*}{dt} + \frac{V_{dc}}{V_{dc}^*}\varsigma_1 i_g - \frac{V_{dc}}{V_{dc}^*}\varsigma_1 i_g^* \tag{19}$$

The effect of parameter mismatch on the behavior of the proposed control strategy can be investigated through a transfer function relating i_g to i_g^*. Hence, ignoring the grid voltage and separating similar terms, one can obtain

$$\frac{V_{dc}}{V_{dc}^*}L_e\frac{di_g^*}{dt} + \frac{V_{dc}}{V_{dc}^*}\varsigma_1 i_g^* = L\frac{di_g}{dt} + \frac{V_{dc}}{V_{dc}^*}\varsigma_1 i_g \tag{20}$$

Taking Laplace transform of (20) and doing some algebraic manipulations, one can obtain the following transfer function

$$G(s) = \frac{I_g(s)}{I_g^*(s)} = \frac{s + \left(\frac{\varsigma_1}{L_e}\right)}{\frac{V_{dc}^* L}{V_{dc} L_e}s + \left(\frac{\varsigma_1}{L_e}\right)} = \frac{s+z}{s+p} \tag{21}$$

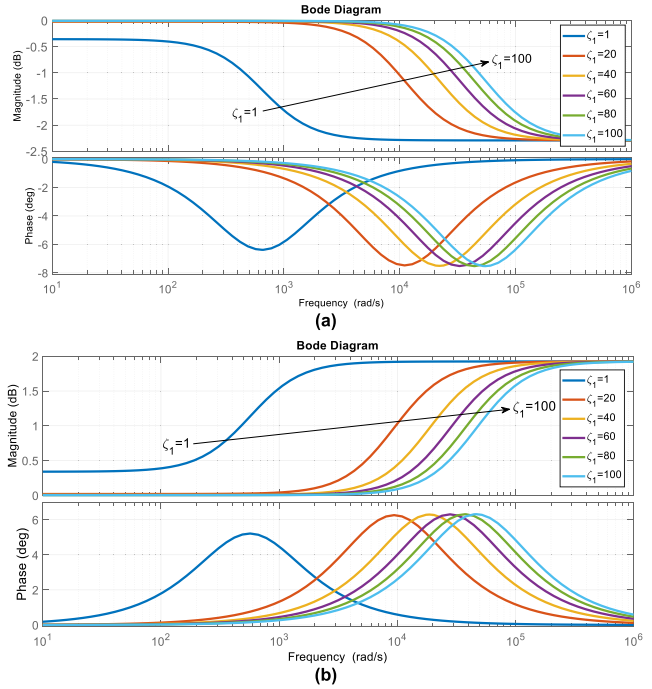

FIGURE 2. Magnitude and phase responses of $G(s)$ for $L_e \neq L$ and $V_{dc} \neq V_{dc}^*$. (a) −20% mismatch, (b) +20% mismatch.

where

$$z = \frac{\varsigma_1}{L_e}, \quad p = \frac{V_{dc}\varsigma_1}{V_{dc}^* L} \tag{22}$$

In the case of parameter mismatch (i.e.: $L_e \neq L$) and $V_{dc} \neq V_{dc}^*$, equation (21) yields different z and p values. When $L_e < L$ and $V_{dc} < V_{dc}^*$, $G(s)$ turns out to be the transfer function of a phase-lag compensator with $z > p$. On the other hand, when $L_e > L$ and $V_{dc} > V_{dc}^*$, $G(s)$ becomes the transfer function of a phase-lead compensator with $z < p$. In both cases, the damping gain ς_1 determines the values of z and p.

The magnitude and phase responses of $G(s)$ obtained by using parameters presented in Table 2 (see Section IV) and various ς_1 values are shown in Fig. 2. Fig. 2(a) shows the magnitude and phase responses for $L_e = 1.6\,\text{mH}$ and $V_{dc} = 240\text{V}$. It can be seen that the magnitude is shifted to the higher frequencies by increasing ς_1. Also, it is attenuated at higher frequencies. On the other hand, the phase is always negative (due to the inherent of phase-lag compensator) and is shifted to the higher frequencies by increasing ς_1. Therefore, a negative phase is added to the phase of reference grid current. Fig. 2(b) shows the magnitude and phase responses for $L_e = 2.4\,\text{mH}$ and $V_{dc} = 260\text{V}$. Again, the magnitude is shifted to the higher frequencies by increasing ς_1. However, unlike the case in Fig. 2(a), the gain is increased at high frequencies. The phase is always positive (due to the inherent of phase-lead compensator) and is shifted to the higher frequencies by increasing ς_1. Hence, a positive phase is added to the phase of reference grid current. The equation of grid current amplitude and its phase in the frequency domain can be written as

$$I_g(j\omega) = |G(j\omega)|\, I_g^*(j\omega) \tag{23}$$

$$\angle I_g(j\omega) = \angle G(j\omega) + \angle I_g^*(j\omega) \tag{24}$$

According to (24), the phase of grid current can be determined by adding individual phases of reference grid current and transfer function $G(j\omega)$. According to Fig. 2, there should be amplitude and phase difference in the grid current for $\varsigma_1 = 1$ at $\omega = 100\pi$ rad/s. According to Fig. 2(a), the grid current with angular frequency $\omega = 100\pi$ rad/s lags its reference when $\varsigma_1 = 1$. On the other hand, according to Fig. 2(b), the grid current with angular frequency $\omega = 100\pi$ rad/s leads its reference when $\varsigma_1 = 1$. However, when ς_1 is sufficiently large ($\varsigma_1 \geq 20$), the amplitude and phase differences in the grid current that would arise due the parameter variations will be compensated. For instance, it is obvious from Fig. 2 that the amplitude and phase differences in the grid current are eliminated ($|G(j\omega)| = 0\,\text{dB}$ and $\angle G(j\omega) \approx 0\,\text{rad/s}$) at $\omega = 100\pi$ rad/s for $\varsigma_1 \geq 20$. This implies that the proposed PBC possesses strong robustness against variations in L. Thus, unlike the PBC strategy presented in [22] and [23], the proposed PBC strategy possesses strong robustness to variations in L.

TABLE 2. System and control parameters.

Description	Value
Grid voltage amplitude, E_m	$120\sqrt{2}$ V
DC-link voltage reference, V_{dc}^*	250V
Inductance, L	2mH
DC capacitors, $C_1 = C_2$	2200μF
Load resistance, R	25Ω, 50Ω, 100Ω
Constant power load (CPL)	2.5kW (max)
Damping gain, ς_1	20
Switching frequency, f_{sw}	4kHz

C. STABILITY STUDY

It is worth noting that the PBC should accomplish the stabilization objective making the closed-loop system passive with an error storage function defined as follows

$$H(x) = \frac{1}{2}Lx_1^2 + \frac{1}{2}Cx_2^2 \tag{25}$$

where $C = C_1C_2/(C_1 + C_2)$. The time derivative of (25) can be written as

$$\dot{H}(x) = x_1 L\dot{x}_1 + x_2 C\dot{x}_2 \tag{26}$$

Substituting (16) and (17) into (26) yields

$$\dot{H}(x) = -\varsigma_1 x_1^2 - (\frac{1}{R_L} + \varsigma_2)x_2^2 \tag{27}$$

It clear from (27) that $\dot{H}(x) < 0$ is always satisfied since $\varsigma_1 > 0$, $\varsigma_2 > 0$, and $R_L > 0$. Therefore, the rectifier system is intrinsically stable because the energy dissipation drives the

error variables (x_1 and x_2) to zero. Equation (25) implies that $H(x) \rightarrow 0, x_1 \rightarrow 0$ and $x_2 \rightarrow 0$.

D. EQUILIBRIUM POINTS

The computation of switching function u in (18) requires the measurements of e_g and i_g, knowledge of L_e, and the generation of i_g^*. Neglecting the switching losses and equating the instantaneous power of ac- and dc-sides, one can obtain

$$\frac{E_m I_m^*}{2} = \frac{V_{dc}^2}{R_L} \tag{28}$$

The reference current amplitude can be computed from (28) as

$$I_m^* = \frac{2V_{dc}^2}{E_m R_L} \tag{29}$$

However, in order to compute I_m^* in (29), the knowledge of R_L is essential. In this study, R_L is estimated using Ohm's law (i.e.: $R_L = V_{dc}/I_L$). The division by zero at the start-up can be prevented if an approximate R_L value is used.

Assuming that $i_g = i_g^*$ ($x_1 = 0$) in the steady-state and substituting (18) into (2), multiplying both sides by V_{dc} and making use of $V_{dc}\frac{dV_{dc}}{dt} = \frac{1}{2}\frac{dV_{dc}^2}{dt}$ and $i_g^*\frac{di_g^*}{dt} = \frac{1}{2}\frac{di_g^{*2}}{dt}$ results in

$$\frac{C_1}{4}\frac{dV_{dc}^2}{dt} + \frac{V_{dc}^2}{R_L} = e_g i_g^* - \frac{L}{2}\frac{di_g^{*2}}{dt} \tag{30}$$

Equation (30) represents the power balance equation of the rectifier from which one can obtain the solution of V_{dc} in the steady-state. Owing to the unity power factor operation, we can consider that $e_g = E_m \sin(\omega t)$ and $i_g^* = I_m^* \sin(\omega t)$. Thus, the terms on the right-hand side of (30) can be written as

$$e_g i_g^* = \frac{E_m I_m^*}{2} - \frac{E_m I_m^*}{2}\cos(2\omega t) \tag{31}$$

$$-\frac{L}{2}\frac{di_g^{*2}}{dt} = -\frac{\omega L I_m^{*2}}{2}\sin(2\omega t) \tag{32}$$

Now, letting new variable $z_1 = V_{dc}^2$ in (30) and making use of equations (31) and (32), the power balance equation can be written as

$$\frac{dz_1}{dt} + \frac{4}{C_1}\frac{z_1}{R_L} = \frac{2E_m I_m^*}{C_1} + \frac{2E_m I_m^*}{C_1}\cos(2\omega t) - \frac{2\omega L I_m^{*2}}{C_1}\sin(2\omega t) \tag{33}$$

Apparently, equation (33) is a first-order differential equation whose solution has a dc component and a double frequency ripple (DFR) component, which is inevitable in single-phase systems.

E. CONTROL OF OUTPUT VOLTAGE

As mentioned before, the regulation of V_{dc} is achieved indirectly provided that $i_g = i_g^*$. Now, assuming that $i_g = i_g^*$ and substituting (18) into (2), we obtain

$$C_1\frac{dV_{C1}}{dt} + \frac{V_{dc}}{R_L} = \frac{E_m I_m^*}{2V_{dc}^*} - \frac{E_m I_m^*}{2V_{dc}^*}\cos(2\omega t) - \frac{L_e}{2V_{dc}^*}\frac{di_g^{*2}}{dt} \tag{34}$$

For the sake of simplicity, we neglect DFR component. Since $V_{C1} = V_{dc}/2$, equation (34) can be written as

$$\frac{dV_{dc}}{dt} + \frac{2V_{dc}}{R_L C_1} = \frac{E_m I_m^*}{V_{dc}^* C_1} \tag{35}$$

Equation (35) is a first-order linear differential equation whose solution is given by

$$V_{dc} = \frac{E_m I_m^* R_L}{2V_{dc}^*} - \frac{E_m I_m^* R_L}{2V_{dc}^*} e^{-(\frac{2}{R_L C_1})t} \tag{36}$$

When the exponential term dies out, V_{dc} converges to

$$V_{dc} = \frac{E_m I_m^* R_L}{2V_{dc}^*} \tag{37}$$

Equation (37) can be written as

$$\frac{V_{dc} V_{dc}^*}{R_L} = \frac{E_m I_m^*}{2} \tag{38}$$

According to (28), (38) is valid if $V_{dc} = V_{dc}^*$. Therefore, this shows that the output voltage control can be achieved indirectly by the proposed PBC.

IV. EXPERIMENTAL VERIFICATION

The effectiveness of the proposed PBC method is investigated experimentally. The block diagram is shown in Fig. 3. The proposed PBC strategy was realized using OPAL-RT OP5600 real-time simulator on the T-type rectifier prototype depicted in Fig. 4. The synchronization with the grid voltage was achieved by using phase-locked loop (PLL). The resistive load and CPL were emulated by using two programmable electronic loads (Chroma-63804), respectively. The grid is emulated via a regenerative grid simulator (Chroma61860). The experimental results were obtained by using the system and control parameters presented in Table 2.

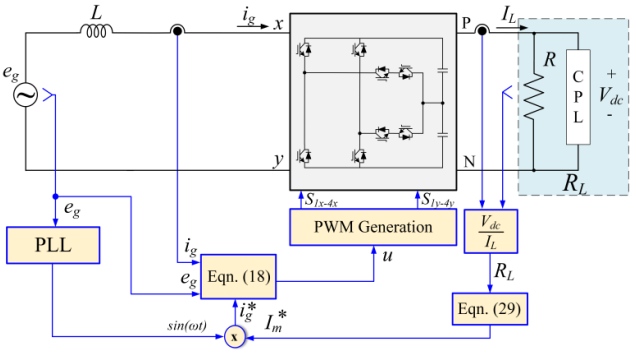

FIGURE 3. Block diagram of the proposed PBC.

A. PERFORMANCE TEST WITH RESISTIVE LOAD

Fig. 5 shows the waveforms of grid voltage (e_g), grid current (i_g) and grid current reference (i_g^*), five-level voltage (v_{xy}), output voltage (V_{dc}) and output voltage reference (V_{dc}^*) and capacitor voltages (V_{C1}, V_{C2}) when the rectifier feeds the resistive load only ($R = 25\Omega$). The system is operated with

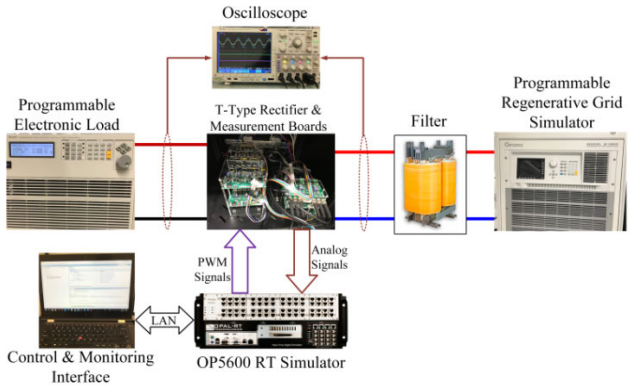

FIGURE 4. Experimental setup.

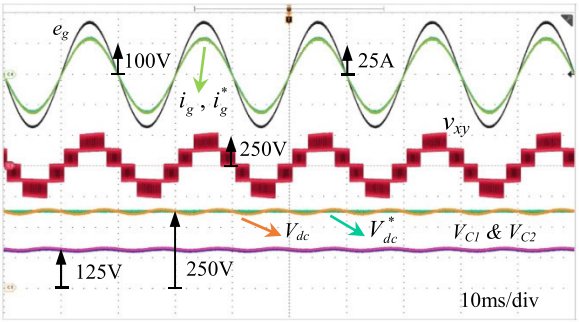

FIGURE 5. Waveforms of grid-voltage (e_g), grid current (i_g) and its reference (i_g^*), five-level voltage (v_{xy}), output voltage (V_{dc}) and its reference (V_{dc}^*), and capacitor voltages (V_{C1} and V_{C2}) under undistorted grid voltage.

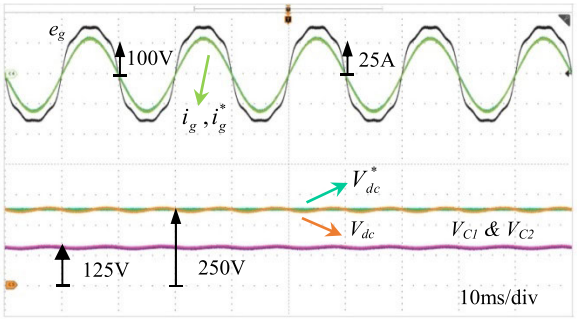

FIGURE 6. Waveforms of grid-voltage (e_g), grid current (i_g) and its reference (i_g^*), output voltage (V_{dc}) and its reference (V_{dc}^*), and capacitor voltages (V_{C1} and V_{C2}) under distorted grid voltage.

$\varsigma_1 = 20$ and $L_e = L$. It is evident that e_g and i_g are in phase with each other which means that the unity power factor operation is satisfied. Also, i_g and i_g^* are overlapped which leads to zero tracking error. The THD of i_g is measured to be 1.3% which is below the recognized standards. The regulation of the output and capacitor voltages is achieved at 250V and 125V, respectively. Obviously, V_{dc} has dc and DFR components as determined analytically in (30). The capacitor voltages are balanced at 125V, which is half of the output voltage. The voltage v_{xy} has five levels +250V, +125V, 0V, −125V and −250V.

Fig. 6 shows operation under distorted grid voltage for $R = 25\Omega$. In the controller, the damping gain is set to 20

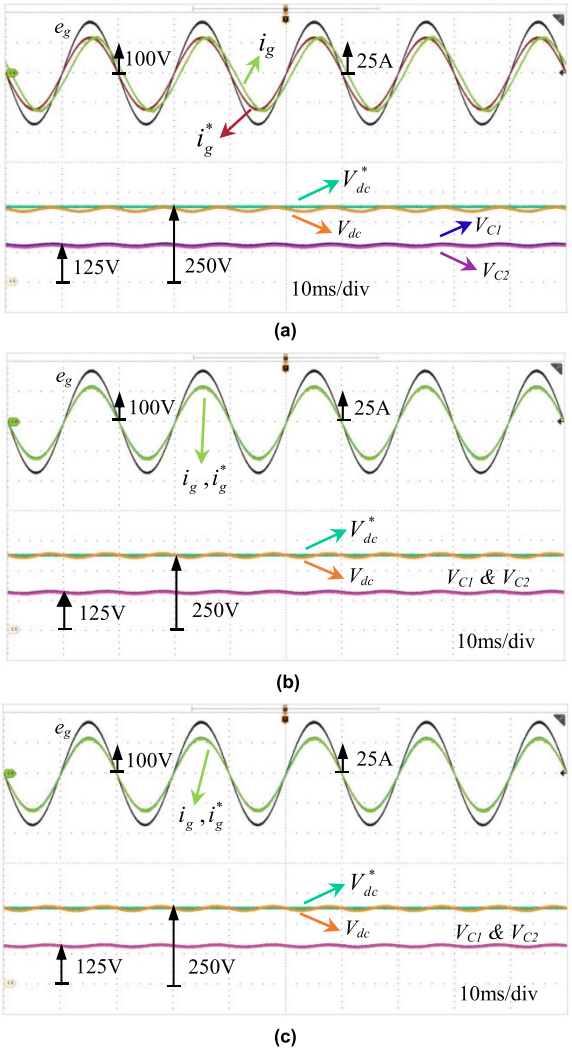

FIGURE 7. Waveforms of grid-voltage (e_g), grid current (i_g) and its reference (i_g^*), output voltage (V_{dc}) and its reference (V_{dc}^*), and capacitor voltages (V_{C1} and V_{C2}) under $R_L = 25\Omega$: (a) $L_e < L$ ($L_e = 1.6$ mH) and $\varsigma_1 = 1$, (b) $L_e < L$ ($L_e = 1.6$ mH) and $\varsigma_1 = 20$, (c) $L_e > L$ ($L_e = 2.4$ mH) and $\varsigma_1 = 20$.

($\varsigma_1 = 20$) and $L_e = L$. In addition to fundamental component at the nominal frequency (50Hz), the distorted grid voltage have additional 3rd, 5th and 7th harmonics with amplitudes $15\sqrt{2}$ V, $7\sqrt{2}$V, and $5\sqrt{2}$V, respectively. Despite the distorted grid voltage, the grid current is almost sinusoidal and in phase with the grid voltage, indicating that the unity power factor requirement is satisfied. The THD of i_g is measured as 2.4%, which meets the required threshold mentioned in [24]. Also, the regulation of V_{dc}, V_{C1} and V_{C2} is achieved at 250V and 125V, respectively.

Fig. 7 shows operation under undistorted grid voltage and $R_L = 25\Omega$ for $L_e < L$ and $L_e > L$. It can be seen from Fig. 7(a) that the output voltage is not regulated at the desired value ($V_{dc} \neq V_{dc}^*$) when $L_e < L$ ($L_e = 1.6$ mH) and $\varsigma_1 = 1$. Such operation is not desired since it causes an unbalance in the capacitor voltages ($V_{C1} \neq V_{C2}$). Also, the grid current lags its reference ($i_g \neq i_g^*$). All of these experimental findings

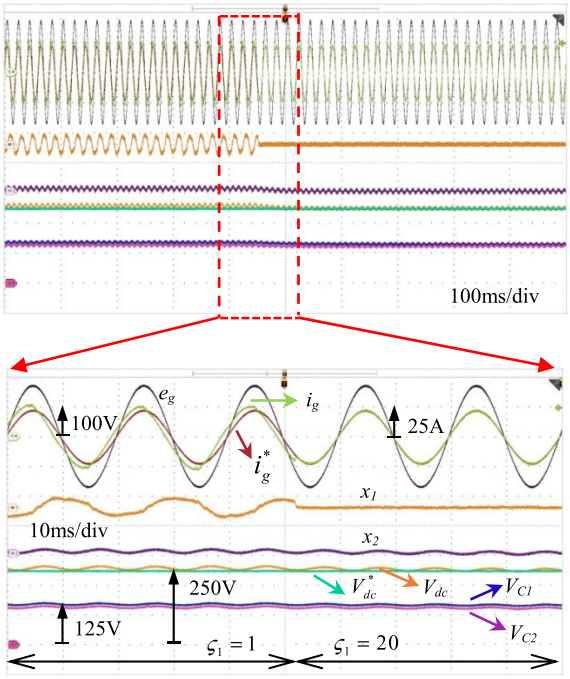

FIGURE 8. Waveforms of grid-voltage (e_g), grid current (i_g) and its reference (i_g^*), output voltage (V_{dc}) and its reference (V_{dc}^*), grid current error (x_1), output voltage error (x_2), and capacitor voltages (V_{C1} and V_{C2}) for a step change in ς_1 from 1 to 20 when $L_e = L$.

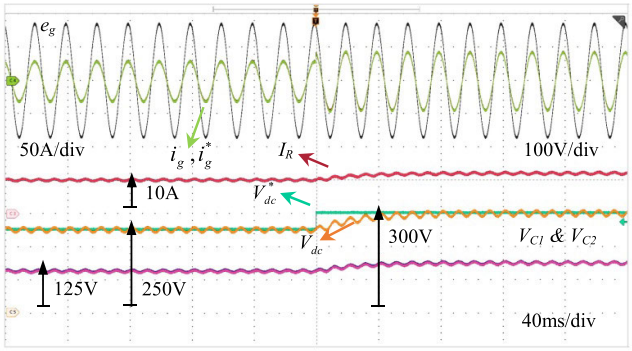

FIGURE 9. Waveforms of grid-voltage (e_g), grid current (i_g) and its reference (i_g^*), output voltage (V_{dc}) and its reference (V_{dc}^*), resistive load current (I_R), and capacitor voltages (V_{C1} and V_{C2}) for a step change in V_{dc}^* from 250V to 300V under resistive load R = 25Ω.

are in good agreement with the theoretical results in Fig. 2(a) and equations (19) and (20). On the other hand, when the damping gain is increased from 1 to 20 ($\varsigma_1 : 1 \rightarrow 20$), these problems have been resolved as shown in Fig. 7(b) and Fig. 7(c). Hence, these results clearly indicate that the proposed PBC has strong robustness against parameter variations in L. In addition, the experimental system was not working at all for $L_e = 2.4\,\text{mH}$ and $\varsigma_1 = 1$ because of the sharp increase in grid current and output voltage which was triggering the protection circuit to stop system. Hence, the effectiveness of the proposed PBC strategy with nonzero damping gain ($\varsigma_1 \neq 0$) can be understood more clearly.

Fig. 8 shows operation under a step change in ς_1 from 0 to 20 for $L_e = L$. Clearly, $i_g \neq i_g^*$, $V_{dc} \neq V_{dc}^*$ and $V_{C1} \neq V_{C2}$ for $\varsigma_1 = 1$. As a consequence of this unsuccessful control,

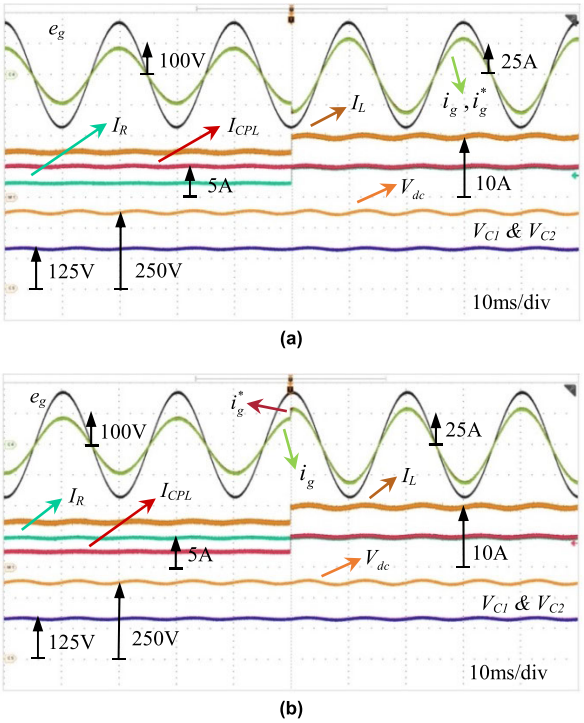

FIGURE 10. Waveforms of grid-voltage (e_g), grid current (i_g) and its reference (i_g^*), output voltage (V_{dc}), resistive load current (I_R), CPL current (I_{CPL}), total load current (I_L), and capacitor voltages (V_{C1} and V_{C2}) for a step change in: (a) R from 100Ω to 50Ω, (b) CPL from 0.625kW to 1.25kW.

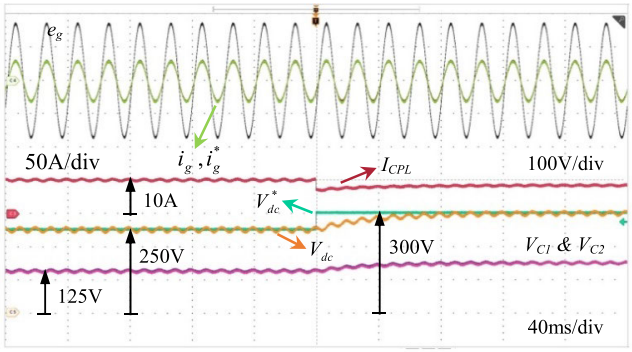

FIGURE 11. Waveforms of grid-voltage (e_g), grid current (i_g) and its reference (i_g^*), output voltage (V_{dc}) and its reference (V_{dc}^*), CPL current (I_{CPL}), and capacitor voltages (V_{C1} and V_{C2}) for a step change in V_{dc}^* from 250V to 300V under CPL.

the error variables are not zero ($x_1 \neq 0$ and $x_2 \neq 0$). Hence, this result verifies the fact that when i_g does not track i_g^*, the control of V_{dc} cannot be accomplished. However, when ς_1 is changed to 20, $i_g = i_g^*$, $V_{dc} = V_{dc}^*$ and $V_{C1} = V_{C2}$. In this case, the error variables eventually tend to zero.

Fig. 9 shows an operation for a step change in V_{dc}^* from 250V to 300V under resistive load $R = 25\Omega$. It is obvious that V_{dc} is regulated at 250V while V_{C1} and V_{C2} are balanced at 125V and i_g is in phase with e_g before and after the step change. It should be noted that the operating point of the rectifier is changed after the step change in V_{dc}^*. Therefore, the amplitude of i_g is increased. After the short transition period, V_{dc} is regulated at 300V. Similarly, V_{C1} and V_{C2} are balanced at 150V.

B. PERFORMANCE TEST WITH RESISTIVE LOAD AND CPL

Fig. 10(a) shows an operation for a step change in R from 100Ω to 50Ω while CPL is maintained at 1.25kW ($R_{CPL} = 50\Omega$).

Even though $R > R_{CPL}$ before the step change, the system is not destabilized. Fig. 10(b) shows an operation for a step change in CPL from 0.625kW to 1.25kW while R is maintained at 50Ω. It can be observed that the control of dc- and ac-side variables is achieved in both tests. That is to say, the grid current tracks its reference and satisfies the unity power factor, and the output voltage is regulated at 250V. The capacitor voltages are balanced at 125V before and after the load change.

Fig. 11 shows an operation for a step change in V_{dc}^* from 250V to 300V when CPL is rated at 2.5kW. It is obvious that V_{dc} is regulated at 250V while V_{C1} and V_{C2} are balanced at 125V and i_g is in phase with e_g before and after the step change. As mentioned in Section II, the CPL exhibits negative resistance characteristics. As a consequence of this fact, in response to the step change in V_{dc}^*, while I_{CPL} reduces from 10A to 8.3A, V_{dc} increases from 250V to 300V. In this case, the load power is maintained constant at 2.5kW.

V. CONCLUSION

This paper presented a robust PBC strategy for single-phase three-level T-type rectifiers feeding resistive and constant power loads. It is pointed out that both dc output voltage and grid current of the rectifier can be controlled if the damping injection is applied to the grid current only. It is shown that the proposed PBC strategy possesses strong robustness to variations in the inductance when the damping gain is selected in accordance with the grid current transfer function magnitude. The performance of the proposed PBC strategy is investigated by experimental studies during steady-state and transients caused by the load and reference voltage changes under undistorted and distorted grid voltage conditions and variations in inductance. It is shown that the dc output voltage is regulated at its reference value, and grid current tracks its reference in all conditions, particularly under constant power load, which may endanger the stability of the system due to the negative resistance characteristic.

REFERENCES

[1] M. P. Kazmierkowski, L. G. Franquelo, J. Rodriguez, M. A. Perez, and J. I. Leon, "High-performance motor drives," *IEEE Ind. Electron. Mag.*, vol. 5, no. 3, pp. 6–26, Sep. 2011.

[2] S. Vazquez, S. M. Lukic, E. Galvan, L. G. Franquelo, and J. M. Carrasco, "Energy storage systems for transport and grid applications," *IEEE Trans. Ind. Electron.*, vol. 57, no. 12, pp. 3881–3895, Dec. 2010.

[3] F. Blaabjerg, M. Liserre, and K. Ma, "Power electronics converters for wind turbine systems," *IEEE Trans. Ind. Appl.*, vol. 48, no. 2, pp. 708–719, Mar./Apr. 2012.

[4] X. Liu, P. C. Loh, P. Wang, and F. Blaabjerg, "A direct power conversion topology for grid integration of hybrid AC/DC energy resources," *IEEE Trans. Ind. Electron.*, vol. 60, no. 12, pp. 5696–5707, Dec. 2013.

[5] G. Wang, G. Konstantinou, C. D. Townsend, J. Pou, S. Vazquez, G. D. Demetriades, and V. G. Agelidis, "A review of power electronics for grid connection of utility-scale battery energy storage systems," *IEEE Trans. Sustain. Energy*, vol. 7, no. 4, pp. 1778–1790, Oct. 2016.

[6] S. Kouro, M. Malinowski, K. Gopakumar, J. Pou, L. G. Franquelo, B. Wu, J. Rodriguez, M. A. Pérez, and J. I. Leon, "Recent advances and industrial applications of multilevel converters," *IEEE Trans. Ind. Electron.*, vol. 57, no. 8, pp. 2553–2580, Aug. 2010.

[7] H. Abu-Rub, J. Holtz, J. Rodriguez, and G. Baoming, "Medium-voltage multilevel converters—State of the art, challenges, and requirements in industrial applications," *IEEE Trans. Ind. Electron.*, vol. 57, no. 8, pp. 2581–2596, Aug. 2010.

[8] M. Schweizer and J. W. Kolar, "Design and implementation of a highly efficient three-level T-type converter for low-voltage applications," *IEEE Trans. Power Electron.*, vol. 28, no. 2, pp. 899–907, Feb. 2013.

[9] M. Malinowski, K. Mozdzynski, T. Gajowik, and S. Stynski, "Fault tolerant smart transformer in distributed energy systems," in *Proc. Conf. Sustain. Energy Supply Energy Storage Syst. (NEIS)*, Hamburg, Germany, Sep. 2019, pp. 15–21.

[10] J.-S. Lee and K.-B. Lee, "An open-switch fault detection method and tolerance controls based on SVM in a grid-connected T-type rectifier with unity power factor," *IEEE Trans. Ind. Electron.*, vol. 61, no. 12, pp. 7092–7104, Dec. 2014.

[11] J. Chen, C. Zhang, X. Xing, and A. Chen, "A fault-tolerant control strategy for T-type three-level rectifier with neutral point voltage balance and loss reduction," *IEEE Trans. Power Electron.*, vol. 35, no. 7, pp. 7492–7505, Jul. 2020.

[12] J. Chen, C. Zhang, A. Chen, X. Xing, and F. Gao, "A carrier-based fault-tolerant control strategy for T-type rectifier with neutral-point voltage oscillations suppression," *IEEE Trans. Power Electron.*, vol. 34, no. 11, pp. 10988–11001, Nov. 2019.

[13] J.-S. Lee, U.-M. Choi, and K.-B. Lee, "Comparison of tolerance controls for open-switch fault in a grid-connected T-type rectifier," *IEEE Trans. Power Electron.*, vol. 30, no. 10, pp. 5810–5820, Oct. 2015.

[14] S. A. Khan, Y. Guo, and J. Zhu, "Model predictive observer based control for single-phase asymmetrical T-type AC/DC power converter," *IEEE Trans. Ind. Appl.*, vol. 55, no. 2, pp. 2033–2044, Mar./Apr. 2019.

[15] Y. Yang, H. Wen, M. Fan, M. Xie, R. Chen, and Y. Wang, "A constant switching frequency model predictive control without weighting factors for T-type single-phase three-level inverters," *IEEE Trans. Ind. Electron.*, vol. 66, no. 7, pp. 5153–5164, Jul. 2019.

[16] S. A. Khan, Y. Guo, Y. P. Siwakoti, D. D.-C. Lu, and J. Zhu, "A disturbance rejection-based control strategy for five-level T-type hybrid power converters with ripple voltage estimation capability," *IEEE Trans. Ind. Electron.*, vol. 67, no. 9, pp. 7364–7374, Sep. 2020.

[17] S. Bayhan and H. Komurcugil, "Sliding-mode control strategy for three-phase three-level T-type rectifiers with DC capacitor voltage balancing," *IEEE Access*, vol. 8, pp. 64555–64564, 2020.

[18] H. Komurcugil and S. Bayhan, "Passivity-based control strategy for single-phase three-level T-type PWM rectifiers," in *Proc. IEEE 29th Int. Symp. Ind. Electron. (ISIE)*, Delft, The Netherlands, Jun. 2020, pp. 1179–1184.

[19] M. Zhang, Y. Li, F. Liu, L. Luo, Y. Cao, and M. Shahidehpour, "Voltage stability analysis and sliding-mode control method for rectifier in DC systems with constant power loads," *IEEE J. Emerg. Sel. Topics Power Electron.*, vol. 5, no. 4, pp. 1621–1630, Dec. 2017.

[20] K. Areerak, T. Sopapirm, S. Bozhko, C. I. Hill, A. Suyapan, and K. Areerak, "Adaptive stabilization of uncontrolled rectifier based AC–DC power systems feeding constant power loads," *IEEE Trans. Power Electron.*, vol. 33, no. 10, pp. 8927–8935, Oct. 2018.

[21] H. Komurcugil, "Improved passivity-based control method and its robustness analysis for single-phase uninterruptible power supply inverters," *IET Power Electron.*, vol. 8, no. 8, pp. 1558–1570, Aug. 2015.

[22] G. Escobar, D. Chevreau, R. Ortega, and E. Mendes, "An adaptive passivity-based controller for a unity power factor rectifier," *IEEE Trans. Control Syst. Technol.*, vol. 9, no. 4, pp. 637–644, Jul. 2001.

[23] D. del Puerto-Flores, J. M. A. Scherpen, M. Liserre, M. M. J. de Vries, M. J. Kransse, and V. G. Monopoli, "Passivity-based control by series/parallel damping of single-phase PWM voltage source converter," *IEEE Trans. Control Syst. Technol.*, vol. 22, no. 4, pp. 1310–1322, Jul. 2014.

HASAN KOMURCUGIL (Senior Member, IEEE) received the B.Sc., M.Sc., and Ph.D. degrees from the Eastern Mediterranean University (EMU), Famagusta, Turkey, in 1989, 1991, and 1998, respectively, all in electrical engineering. From 2004 to 2010, he was the Head of the Department of Computer Engineering, EMU. In 2010, he played an active role in preparing the department's first self-study report for the use of Accreditation Board for Engineering and Technology. In 2010, he was elected as the Board Member of Higher Education, Planning, Evaluation, Accreditation and Coordination Council (YODAK), North Cyprus. From 2010 to 2019, he played active role in evaluating the universities in North Cyprus. He is currently a full-time Professor with the Department of Computer Engineering, EMU. He is a coauthor of one book chapter. His research interests include power electronics and innovative control methods for power converters. He was a recipient of the Best Presentation Recognitions at the 41st and 42nd Annual Conferences of the IEEE Industrial Electronics Society, in 2015 and 2016, respectively. He is a member of the IEEE Industrial Electronics Society. He is also the Chair of the Renewable Energy Systems Subcommittee of Power Electronics Technical Committee of IES. He served as the Corresponding Guest Associate Editor for the IEEE TRANSACTIONS ON ENERGY CONVERSION and the Guest Editor for the IEEE TRANSACTIONS ON INDUSTRIAL INFORMATICS. He also serves as an Associate Editor for the IEEE TRANSACTIONS ON INDUSTRIAL ELECTRONICS and the IEEE TRANSACTIONS ON INDUSTRIAL INFORMATICS.

SERTAC BAYHAN (Senior Member, IEEE) received the M.S. and Ph.D. degrees in electrical engineering from Gazi University, Ankara, Turkey, in 2008 and 2012, respectively. His undergraduate studies also at the same university and he graduated as valedictorian.

In 2008, he joined the Department of Electronics and Automation, Gazi University, as a Lecturer, where he was promoted to an Associate Professor, in 2017. From 2014 to 2018, he worked at Texas A&M University, Qatar, as an Associate Research Scientist. He is currently working with the Qatar Environment and Energy Research Institute (QEERI), as a Senior Scientist, and he is the Faculty Member with the rank of Associate Professor with the Sustainable Division of College of Science and Engineering, Hamad Bin Khalifa University. He has acquired $13M in research funding and published more than 150 papers in mostly prestigious IEEE journals and conferences. He is also the coauthor of two books and five book chapters.

Dr. Bayhan was a recipient of many prestigious international awards, such as the Research Fellow Excellence Award in recognition of his research achievements and exceptional contributions to the Texas A&M University, Qatar, in 2018, the Best Paper Presentation Recognition at the 41st and 42nd Annual Conference of the IEEE Industrial Electronics Society, in 2015 and 2016, respectively, Research Excellence Travel Awards in 2014 and 2015 (Texas A&M University at Qatar), and the Researcher Support Award from the Scientific and Technological Research Council of Turkey (TUBITAK). Because of the visibility of his research, he has been recently elected as the Chair of IES Power Electronics Technical Committee. He is also serves as an Associate Editor for IEEE TRANSACTIONS ON INDUSTRIAL ELECTRONICS, IEEE JOURNAL OF EMERGING AND SELECTED TOPICS IN INDUSTRIAL ELECTRONICS, IEEE OPEN JOURNAL OF THE INDUSTRIAL ELECTRONICS SOCIETY, and IEEE INDUSTRIAL ELECTRONICS TECHNOLOGY NEWS, and the Guest Editor for the IEEE TRANSACTIONS ON INDUSTRIAL INFORMATICS.

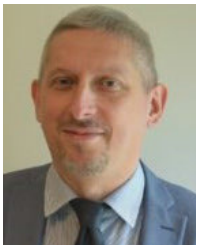

MARIUSZ MALINOWSKI (Fellow, IEEE) received the Ph.D. and D.Sc. degrees in electrical engineering from the Institute of Control and Industrial Electronics, Warsaw University of Technology (WUT), Warsaw, Poland, in 2001 and 2012, respectively. He was a Visiting Scholar with Aalborg University, Aalborg, Denmark; the University of Nevada, Reno, NV, USA; the Technical University of Berlin, Berlin, Germany; and ETH Zürich, Zürich, Switzerland. He is currently with the Institute of Control and Industrial Electronics, WUT. He has coauthored over 150 technical articles and six books. His current research interests include the control and the modulation of grid-side converters, multilevel converters, smart grids, and power-generation systems based on renewable energies. He was a recipient of the Siemens Prize, in 2002 and 2007; the WUT President Scientific Prize, in 2015; the Polish Minister of Science and the Higher Education Awards, in 2003 and 2008, respectively; the Prime Minister of Poland Award for Habilitation, in 2013; and the IEEE Industrial Electronics Society (IES) David Irwin Early Career Award, in 2011, and the Bimal Bose Energy Systems Award, in 2015. His industry application received several awards and medals.